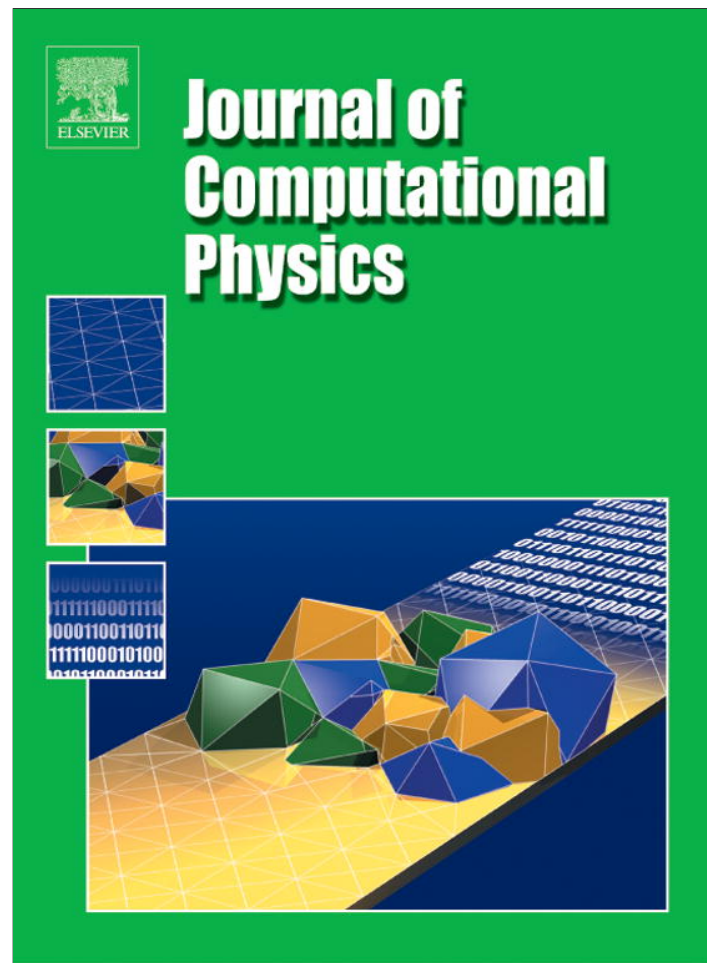


Provided for non-commercial research and education use.
Not for reproduction, distribution or commercial use.



(This is a sample cover image for this issue. The actual cover is not yet available at this time.)

This article appeared in a journal published by Elsevier. The attached copy is furnished to the author for internal non-commercial research and education use, including for instruction at the authors institution and sharing with colleagues.

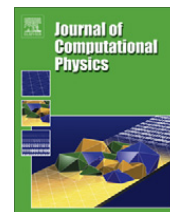
Other uses, including reproduction and distribution, or selling or licensing copies, or posting to personal, institutional or third party websites are prohibited.

In most cases authors are permitted to post their version of the article (e.g. in Word or Tex form) to their personal website or institutional repository. Authors requiring further information regarding Elsevier's archiving and manuscript policies are encouraged to visit:

<http://www.elsevier.com/copyright>

Contents lists available at [SciVerse ScienceDirect](#)

Journal of Computational Physics

journal homepage: www.elsevier.com/locate/jcp

Modeling and simulations of drop pinch-off from liquid crystal filaments and the leaky liquid crystal faucet immersed in viscous fluids



Xiaofeng Yang^{a,*}, M. Gregory Forest^b, Huiyuan Li^c, Chun Liu^d, Jie Shen^e, Qi Wang^a, Falai Chen^f

^a Department of Mathematics, University of South Carolina, Columbia, SC 29083, USA

^b Department of Mathematics, Institute for Advanced Materials, Nanoscience & Technology, University of North Carolina at Chapel Hill, Chapel Hill, NC 27599-3250, USA

^c Institute of Software, Chinese Academy of Sciences, Beijing 100090, China

^d Department of Mathematics, Pennsylvania State University, University Park, PA 16802, USA

^e Department of Mathematics, Purdue University, West Lafayette, IN 47907, USA

^f Department of Mathematics, University of Science and Technology of China, Hefei, Anhui 230026, China

ARTICLE INFO

Article history:

Received 26 December 2011

Received in revised form 22 October 2012

Accepted 26 October 2012

Available online 3 December 2012

Keywords:

Phase field model

Drop pinch-off

Liquid crystal filament

ABSTRACT

An energy-based, phase field model is developed for the coupling of two incompressible, immiscible complex fluid phases, in particular a nematic liquid crystal phase in a viscous fluid phase. The model consists of a system of coupled nonlinear partial differential equations for conservation of mass and momentum, phase transport, and interfacial boundary conditions. An efficient and easy-to-implement numerical scheme is developed and implemented to extend two benchmark fluid mechanical problems to incorporate a liquid crystal phase: filament breakup under the influence of capillary force and the gravity-driven, dripping faucet. We explore how the distortional elasticity and nematic anchoring at the liquid crystal-air interface modify the capillary instability in both problems. For sufficiently weak distortional elasticity, the effects are perturbative of viscous fluid experiments and simulations. However, above a Frank elasticity threshold, the model predicts a transition to the beads-on-a-string phenomenon associated with polymeric fluid filaments.

Published by Elsevier Inc.

1. Introduction

Complex fluids require some description of internal microstructure to accurately predict and understand their behavior, cf. [29] and references therein. Complex fluids abound in Nature as well as in synthetic and engineered materials where the microstructure can be manipulated by flow and deformation to produce useful mechanical, chemical, optical or thermal properties. Often, complex fluids reside next to or are immersed in another fluid phase. The modeling of *complex fluid mixtures in free surface flows* presents a new level of complexity, where the simulation of complex constitutive laws for fluid microstructure is coupled to free surfaces between fluid phases that undergo topological changes and singularities. In this paper, we are specifically interested in binary mixtures of incompressible, immiscible fluid components where one phase is a nematic liquid crystal and the other phase is a viscous fluid.

* Corresponding author.

E-mail addresses: xfyang@math.sc.edu (X. Yang), forest@unc.edu (M. Gregory Forest), huiyuan@iscas.ac.cn (H. Li), liu@math.psu.edu (C. Liu), shen@math.purdue.edu (J. Shen), qwang@math.sc.edu (Q. Wang), chenfl@ustc.edu.cn (F. Chen).

In engineering applications, mixtures or composites of immiscible viscous fluid phases have been extensively explored, cf. the now classical reviews by Rallison [46] and Stone [56], more recently the special issue of *Lab on a Chip* [1], and in particular the review by Cristini and Tan [13] and references therein. A generic application is to use microfluidic devices to tune drop size distributions. In these multi-phase processes, immiscible components are separated by free interfaces that transport and deform depending on the initial data and flow processing conditions. The interfacial physics, material properties, and coupling to the relevant flow conditions determine the dynamics of each fluid phase and any interfacial singularities [23].

Here we focus on a close cousin of the above two-phase viscous fluid experiments where liquid crystal (LC) domains (filaments, droplets) are dispersed in an immiscible fluid phase (viscous for this study), and then driven through topological transitions (drop pinch-off). We are specifically interested in the coupling between capillary and gravity forces in liquid crystal filaments immersed in a viscous fluid phase, and the subsequent breakup of the LC filament. The shear rupture of LC droplets immersed in a viscous fluid, the analog of the topic reviewed by Rallison [46], was previously studied by the authors using a phase field model [63] that is generalized here as discussed in Section 2.

The modeling of a LC filament in a viscous fluid is also a close cousin to the classical problem of viscous fluid filament breakup in air and the Rayleigh instability, its generalization to viscoelastic (complex) fluid filaments in air, and replacement of the ambient air with another viscous or complex fluid phase. The disparities, experimentally and numerically, between viscous filament dynamics in air and viscoelastic or complex fluid filament dynamics in air, are well documented in the literature, cf. [6,49] and references therein. One of the most striking viscoelastic filament phenomena is the so-called "beads-on-a-string" (BOAS) morphology that forms during breakup, which has been numerically explored primarily with one-dimensional *ad hoc* asymptotic models (cf. [6,49] and references therein), with the notable exception of the axisymmetric three-dimensional simulations of viscoelastic inkjet printing by Morrison and Harlen [40].

Complex fluid models usually expand the Navier–Stokes equation by introducing an extra stress (beyond the viscous stress and pressure) as a functional of the microstructure, and then there is a separate transport equation specific to the microstructure. There are choices to be made as to what level of detail is required to resolve the microstructure. In this paper, we use a simplified Leslie–Ericksen continuum director theory to describe the orientation of liquid crystal molecules and the coupling between the LC microstructure and hydrodynamics [30,18,7].

For the two-phase liquid crystal and viscous fluid system, the interfacial domain between the immiscible liquid crystal and viscous fluid phases must be modeled. Numerical approaches to simulate free surfaces between phases can be divided into interface tracking versus interface capturing methods. The primary distinction between these two numerical approaches lies in whether the mesh evolves with the interface or the interface evolves through and without regard to the mesh. Typical interface tracking techniques include boundary integral methods [25,59], front tracking [20,58], and the immersed boundary method [45], whereas interface capturing methods include volume-of-fluid (VOF) methods [24,28], the level-set method [44,3], lattice Boltzmann and lattice gas methods [47,10,41,60,48,2], and the diffuse interface (equivalently, phase field) approach [39,38,4] in which the interface is spread into a finite transition layer where the two fluids mix to a certain degree, governed by a prescribed mixing energy. The length scale defined by the transition layer is normally smaller than the length scale of resolution in the bulk fluid domain. The leading order description of the transition layer in terms of the length scale ratio between the transition layer and the bulk is the sharp interface limit. In this regard, the diffuse interface description of the interfacial problem is more detailed and, if modeled correctly, can include more detailed interfacial physics than sharp interfaces with a prescribed surface tension.

The governing equations in the phase field model arise from a standard energetic variational procedure including the Hamilton least action principle (for reversible processes) and the Onsager maximum dissipation principle (for irreversible processes) [42,43,8,22,4,39]. For liquid crystals, energy potentials are well studied for near equilibrium conditions and have been coupled to hydrodynamics in the past.

In this paper, we explore an immiscible liquid crystal phase (initially a filament) immersed in a viscous fluid, and simulate the dynamics during the formation of interfacial singularities (in terms of thin threads connecting beads which pinch-off into drops). We derive a phase-field model that couples with the free boundary between phases, hydrodynamics of the mixture, and the orientational field of the LC microstructure. The model extends our previous results [64,63] in that (i) the new model satisfies an energy dissipation law; and (ii) the Cahn–Hilliard transport equation for the phase variable is replaced by an Allen–Cahn transport equation with a Lagrange multiplier to conserve mass. The second feature reduces computational complexity from the Cahn–Hilliard equation arising from higher order spatial derivatives. This choice is shown to produce a more robust and better resolved interface for these interfacial problems. In this new numerical scheme, we combine several effective numerical approaches which have proven efficient for the phase transport equations coupled with the Navier–Stokes equations, namely, stabilized schemes (cf. [62,55,54,53]) for the phase transport equations and projection-type schemes [21] for the Navier–Stokes equations. We simulate 3-D, axisymmetric LC filament stretching and pinch-off into drops under the influence of surface tension and gravity. The code is first benchmarked on viscous fluid filaments and then used to study LC filaments. In the numerical experiments on LC filaments, the role of distortional elasticity and the anchoring strength in facilitating or retarding the interfacial singularity formation is conducted. In the regime of strong distortional elasticity, satellite droplets connected by thin threads are shown, which resembles the beads-on-the-string phenomenon observed in liquid filaments of flexible polymer solutions under capillary forces. The mechanisms leading to this phenomenon in LCs are distortional elasticity and surface anchoring rather than chain stretching, recoiling and relaxation in flexible polymer solutions.

The remainder of the paper is organized as follows. In Section 2, we derive the phase field model for the two phase complex fluid system and establish the energy dissipation law following a variational method. In Section 3, we develop the numerical method for the phase field model system, employing several techniques which are particularly suitable for the interfacial problem studied. In Section 4, we present numerical results for two benchmark problems: singularity formation in cylindrical filaments of liquid crystals subject to capillary forces and drop pinch-off in liquid crystal filament flows under the influence of gravity.

2. The phase field formulation of two-phase complex fluids

We consider a mixture of two immiscible, incompressible fluids with densities ρ_1, ρ_2 and viscosities ν_1, ν_2 , respectively. To distinguish distinct fluid phases, a dynamical phase field variable or labeling function ϕ is introduced:

$$\phi(\mathbf{x}, t) = \begin{cases} 1 & \text{fluid1} \\ -1 & \text{fluid2.} \end{cases} \quad (2.1)$$

In the phase field description of binary fluids, the phase field or labeling function is required to be differentiable so that a thin smooth transition layer of thickness ϵ connects the two pure fluid phases. The “interface” is simply declared as the zero level set of the labeling function, $\Gamma_t = \{\mathbf{x} : \phi(\mathbf{x}, t) = 0\}$, whereas in the pure phases the phase field function typically has constant values $+1, -1$, respectively. In order to force the value of the phase variable to be ± 1 within the pure phases, we employ a Ginzburg–Landau double-well potential: $F(\phi) = \frac{1}{4\epsilon^2}(\phi^2 - 1)^2$, where ϵ is a parameter proportional to the thickness of the interface. The mixing energy functional is given by

$$E_{\text{mix}} = \int_{\Omega} W_{\text{mix}}(\phi, \nabla\phi) d\mathbf{x} = \int_{\Omega} \lambda \left(\frac{1}{2} |\nabla\phi|^2 + F(\phi) \right) d\mathbf{x}, \quad (2.2)$$

which represents the competition between the hydrophilic and hydrophobic properties of the two fluids, where $W_{\text{mix}} = \lambda(\frac{1}{2}|\nabla\phi|^2 + F(\phi))$ is the mixing energy density, and λ parametrizes the magnitude of mixing energy that also incorporates the surface tension.

We consider the binary fluid of liquid crystals and viscous fluids and use $\phi = 1$ to denote the nematic liquid crystal phase. For the nematic liquid crystal phase, we use the standard Oseen–Frank distortional energy density for the bulk free energy [17,30,18],

$$W_{\text{bulk}}(\mathbf{d}) = \frac{1}{2}K_1(\nabla \cdot \mathbf{d})^2 + \frac{1}{2}K_2(\mathbf{d} \cdot \nabla \times \mathbf{d})^2 + \frac{1}{2}K_3(\mathbf{d} \times \nabla \times \mathbf{d})^2, \quad (2.3)$$

where the unit vector \mathbf{d} represents the average orientation of liquid crystal molecules and K_1, K_2, K_3 are elastic constants for the three canonical distortional modes: splay, twist and bend. For simplicity, we suppress the anisotropic distortional elastic modes by assuming $K_1 = K_2 = K_3 = K$. Then, the Oseen–Frank energy density reduces to the Dirichlet functional $\frac{K}{2}|\nabla\mathbf{d}|^2$ modulo the null-Lagrangian term which is determined by the boundary anchoring of the director [11,14,33,12]. Moreover, rather than imposing a norm 1 constraint directly on \mathbf{d} , we introduce a penalty term of the Ginzburg–Landau type $G(\mathbf{d}) = \frac{1}{4\eta^2}(|\mathbf{d}|^2 - 1)^2$ to regularize the distortional energy in the cores of topological defects [18,31–34], where η is a penalization parameter that is proportional to the size of the defect core (or zone). This regularization allows the free energy to be finite at the defect core, extending the classical Ericksen–Leslie model to handle liquid crystal flows where defects are created and annihilated in time and space. Then, the regularized elastic bulk energy density is given by

$$W_{\text{bulk}}(\mathbf{d}, \nabla\mathbf{d}) = K \left(\frac{|\nabla\mathbf{d}|^2}{2} + G(\mathbf{d}) \right). \quad (2.4)$$

At the interface between liquid crystal and another material phase, liquid crystals prefer some orientation known as the easy (anchoring) direction. There are two types of most commonly used anchoring conditions: planar (or parallel) anchoring, where all directions in the plane of the interface are easy directions, and homeotropic (or normal) anchoring, where the easy direction is the normal to the interface [27,14,26,66,64]. The anchoring condition can be modeled using a surface free energy functional called the anchoring energy. We proposed an anchoring energy density that can accommodate both the parallel and homeotropic anchoring as follows

$$W_{\text{anch}}(\phi, \nabla\phi, \mathbf{d}, \nabla\mathbf{d}) = \begin{cases} \frac{A}{2} |\mathbf{d} \cdot \nabla\phi|^2, & \text{parallel,} \\ \frac{A}{2} (|\mathbf{d}|^2 |\nabla\phi|^2 - |\mathbf{d} \cdot \nabla\phi|^2), & \text{homeotropic,} \end{cases} \quad (2.5)$$

where $A = A(x)$ parametrizes the strength of the anchoring energy. We obtain the total energy of the hydrodynamic system as a sum of the kinetic energy E_{kin} , the mixing energy E_{mix} , the bulk energy E_{bulk} , and the anchoring energy E_{anch} [64,19,65]:

$$\mathcal{E}_{\text{tot}} = E_{\text{kin}} + E_{\text{mix}} + \left(\frac{1+\phi}{2} \right)^2 E_{\text{bulk}} + E_{\text{anch}} = \int_{\Omega} \left(\frac{1}{2} \rho |\mathbf{u}|^2 + W_{\text{mix}}(\phi, \nabla\phi) + \left(\frac{1+\phi}{2} \right)^2 W_{\text{bulk}} + W_{\text{anch}} \right) d\mathbf{x}, \quad (2.6)$$

where ρ is the density, \mathbf{u} is the fluid velocity field, the factor $\left(\frac{1+\phi}{2}\right)^2$ represents the volume fraction of the nematic liquid crystal component, which vanishes in the viscous liquid phase ($\phi = -1$). In general, for a nematic liquid, the viscous stress is anisotropic and depends on the LC orientation. For simplicity, we use a viscous stress $\sigma_{\text{vis}} = v \left(\frac{\nabla \mathbf{u} + (\nabla \mathbf{u})^T}{2} \right)$ in both components where $v = v_1 \phi + (1 - \phi)v_2$ is the viscosity for the mixture. If one assumes a generalized Fick's law that the mass flux be proportional to the gradient of the chemical potential [9,36,35], we derive the following governing system of equations:

$$\phi_t + (\mathbf{u} \cdot \nabla)\phi = -M_1 \frac{\delta \mathcal{E}_{\text{tot}}}{\delta \phi}, \quad (2.7)$$

$$\mathbf{d}_t + (\mathbf{u} \cdot \nabla)\mathbf{d} - \mathbf{W} \cdot \mathbf{d} = -M_2 \frac{\delta \mathcal{E}_{\text{tot}}}{\delta \mathbf{d}}, \quad (2.8)$$

$$\rho(\mathbf{u}_t + (\mathbf{u} \cdot \nabla)\mathbf{u}) + \nabla p = \nabla \cdot (\sigma_{\text{vis}} + \sigma_{\text{mix}}^e + \sigma_{\text{bulk}}^e + \sigma_{\text{anch}}^e + \sigma_{\text{asym}}^e), \quad (2.9)$$

$$\nabla \cdot \mathbf{u} = 0, \quad (2.10)$$

where p is the hydrostatic pressure, M_1^{-1} is the relaxation parameter for the phase function, M_2^{-1} is the relaxation parameter of the liquid crystal, σ_{mix}^e , σ_{bulk}^e , σ_{anch}^e are the corresponding elastic stress tensors derived from each energy components by the least action principle, respectively [8,33–35,5], and $\sigma_{\text{asym}}^e = \frac{1}{2} \left(\frac{\delta \mathcal{E}_{\text{tot}}}{\delta \mathbf{d}} \mathbf{d} - \mathbf{d} \frac{\delta \mathcal{E}_{\text{tot}}}{\delta \mathbf{d}} \right)$ is the asymmetric elastic stress corresponding to the invariant time derivative in \mathbf{d} , where \mathbf{W} is the vorticity tensor. The variational derivative $\frac{\delta \mathcal{E}_{\text{tot}}}{\delta \phi}$ can be taken in H^{-1} , leading to the (conserved) Cahn–Hilliard phase transport equation,

$$\phi_t + (\mathbf{u} \cdot \nabla)\phi = -M_1 \Delta \mu, \quad (2.11)$$

$$\mu = \lambda(\Delta \phi - f(\phi)) - K \left(\frac{1+\phi}{2} \right) \left(\frac{|\nabla \mathbf{d}|^2}{2} + G(\mathbf{d}) \right) - A \nabla \cdot ((\nabla \phi \cdot \mathbf{d})\mathbf{d}), \quad (2.12)$$

with the boundary conditions $\partial_n \phi|_{\partial \Omega} = 0$ and $\partial_n \Delta \phi|_{\partial \Omega} = 0$ where $f(\phi) = F'(\phi)$ and n is the outward normal direction. In this case, M_1 is called the mobility parameter. Alternatively, taking the variational derivative in L^2 , we obtain the Allen–Cahn phase transport equation

$$\phi_t + (\mathbf{u} \cdot \nabla)\phi = M_1 \mu, \quad (2.13)$$

with the boundary condition $\partial_n \phi|_{\partial \Omega} = 0$. We note that the Allen–Cahn equation does not conserve the total volume. So, to conserve the volume of the liquid crystal phase in the mixture, we have to augment the energy functional by a Lagrangian term proportional to $\int \phi d\mathbf{x}$.

In this paper, we adopt the Allen–Cahn model for simplicity. We remark that all the analytical and numerical work can be generalized to the Cahn–Hilliard model without additional difficulties (cf. [55,54,53]). In general, the liquid crystal component and the host viscous fluid matrix do not have the same density and viscosity, but for this paper we assume there are no contrasts, $\rho_1 = \rho_2$ and $v_1 = v_2 = v$. The resulting system of equations is summarized as follows:

$$\phi_t + (\mathbf{u} \cdot \nabla)\phi = M_1 \lambda(\Delta \phi - f(\phi)) - M_1 K \left(\frac{1+\phi}{2} \right) \left(\frac{|\nabla \mathbf{d}|^2}{2} + G(\mathbf{d}) \right) - M_1 A \mathcal{A}_\phi, \quad (2.14)$$

$$\mathbf{d}_t + (\mathbf{u} \cdot \nabla)\mathbf{d} - \mathbf{W} \cdot \mathbf{d} = M_2 K \left(\nabla \cdot \left(\frac{1+\phi}{2} \right)^2 \nabla \mathbf{d} - \left(\frac{1+\phi}{2} \right)^2 g(\mathbf{d}) \right) - M_2 A \mathcal{A}_\mathbf{d}, \quad (2.15)$$

$$\mathbf{u}_t + (\mathbf{u} \cdot \nabla)\mathbf{u} - \nu \Delta \mathbf{u} + \nabla p + \nabla \cdot (\lambda \nabla \phi \otimes \nabla \phi + K \left(\frac{1+\phi}{2} \right)^2 \nabla \mathbf{d} \otimes \nabla \mathbf{d}) \quad (2.16)$$

$$- \frac{K}{2} \left(\nabla \cdot \left(\frac{1+\phi}{2} \right)^2 \nabla \mathbf{d} \otimes \mathbf{d} - \mathbf{d} \otimes \nabla \cdot \left(\frac{1+\phi}{2} \right)^2 \nabla \mathbf{d} \right) + A \mathcal{A}_\mathbf{u} = 0, \quad (2.17)$$

$$\nabla \cdot \mathbf{u} = 0, \quad (2.18)$$

$$\mathbf{u}|_{\partial \Omega} = 0, \quad \partial_n \phi|_{\partial \Omega} = 0, \quad \partial_n \mathbf{d}|_{\partial \Omega} = 0. \quad (2.19)$$

where

$$\mathcal{A}_\phi = \begin{cases} \nabla \cdot ((\nabla \phi \cdot \mathbf{d})\mathbf{d}), & \text{parallel,} \\ \nabla \cdot (|\mathbf{d}|^2 \nabla \phi - (\nabla \phi \cdot \mathbf{d})\mathbf{d}), & \text{homeotropic,} \end{cases} \quad (2.20)$$

$$\mathcal{A}_{\mathbf{d}} = \begin{cases} (\mathbf{d} \cdot \nabla \phi) \nabla \phi, & \text{parallel,} \\ (\nabla \phi \cdot \nabla \phi) \mathbf{d} - (\mathbf{d} \cdot \nabla \phi) \nabla \phi, & \text{homeotropic,} \end{cases} \quad (2.21)$$

$$\mathcal{A}_{\mathbf{u}} = \begin{cases} (\mathbf{d} \cdot \nabla \phi) \mathbf{d} \otimes \nabla \phi, & \text{parallel,} \\ ((\mathbf{d} \cdot \mathbf{d}) \nabla \phi - (\mathbf{d} \cdot \nabla \phi) \mathbf{d}) \otimes \nabla \phi, & \text{homeotropic,} \end{cases} \quad (2.22)$$

$$g(\mathbf{d}) = G'(\mathbf{d}).$$

We solve the system of equations in a regular computational domain. The velocity boundary condition is no-slip; for the phase variable ϕ and the liquid crystal orientational director \mathbf{d} , we assume the volume flux and director flux vanishes at solid walls leading to the Neumann boundary condition for ϕ and \mathbf{d} [62,35,64,52]. The boundary conditions for these hydrodynamical variables can be either periodic or physical, whereas here we adopt physical boundary conditions.

It can be readily established that the total energy of the system (3.1)–(3.5) is dissipative. Specifically, if we take the inner product of (3.1) with $\frac{\delta \mathcal{E}_{\text{tot}}}{\delta \phi}$ (3.2) with $\frac{\delta \mathcal{E}_{\text{tot}}}{\delta \mathbf{d}}$, and (3.4) with \mathbf{u} , and then sum up all the equalities, we obtain the energy dissipation law as follows

$$\partial_t \mathcal{E}_{\text{tot}} = - \int_{\Omega} \left(\nu |\nabla \mathbf{u}|^2 + M_1 \left| \frac{\delta \mathcal{E}_{\text{tot}}}{\delta \phi} \right|^2 + M_2 \left| \frac{\delta \mathcal{E}_{\text{tot}}}{\delta \mathbf{d}} \right|^2 \right) d\mathbf{x}. \quad (2.23)$$

Then, one can prove the existence and uniqueness of the weak solution with certain smoothness by a standard Galerkin procedure [16].

We remark that a similar but simplified model system has been used previously [64,19,65,63]. However, several nonlinear coupling terms are omitted for simplicity in those studies so that the energy dissipation law (2.23) was not established.

3. Nondimensionalization

We introduce a characteristic length and time scale L and t_0 , respectively, to nondimensionalize space and time variable, $\tilde{\mathbf{x}} = \frac{\mathbf{x}}{L}$, $\tilde{t} = \frac{t}{t_0}$, respectively. The dimensionless velocity is then defined by $\tilde{\mathbf{u}} = \frac{\mathbf{u} t_0}{h}$ and the pressure by $\tilde{p} = \frac{p t_0^2}{L^2 \rho}$. By definition, ϕ and \mathbf{d} are dimensionless variables already. The dimensionless governing system of equations is summarized as follows

$$\phi_t + (\mathbf{u} \cdot \nabla) \phi = \frac{\tilde{M}_1}{Ca} (\Delta \phi - \tilde{f}(\phi)) - \frac{\tilde{M}_1}{Er} \left(\frac{1 + \phi}{2} \right) \left(\frac{|\nabla \mathbf{d}|^2}{2} + \tilde{G}(\mathbf{d}) \right) - \tilde{M}_1 \tilde{A} \mathcal{A}_{\phi}, \quad (3.1)$$

$$\mathbf{d}_t + (\mathbf{u} \cdot \nabla) \mathbf{d} - \mathbf{W} \cdot \mathbf{d} = \frac{\tilde{M}_2}{Er} \left(\nabla \cdot \left(\frac{1 + \phi}{2} \right)^2 \nabla \mathbf{d} - \left(\frac{1 + \phi}{2} \right)^2 \tilde{g}(\mathbf{d}) \right) - \tilde{M}_2 \tilde{A} \mathcal{A}_{\mathbf{d}}, \quad (3.2)$$

$$[\mathbf{u}_t + (\mathbf{u} \cdot \nabla) \mathbf{u}] - \frac{1}{Re} \Delta \mathbf{u} + \nabla p + \frac{1}{Re} \nabla \cdot \left(\frac{1}{Ca} \nabla \phi \otimes \nabla \phi + \frac{1}{Er} \left(\left(\frac{1 + \phi}{2} \right)^2 \nabla \mathbf{d} \otimes \nabla \mathbf{d} \right. \right. \quad (3.3)$$

$$\left. \left. + \frac{1}{2} \left(\nabla \cdot \left(\frac{1 + \phi}{2} \right)^2 \nabla \mathbf{d} \otimes \mathbf{d} - \mathbf{d} \otimes \nabla \cdot \left(\frac{1 + \phi}{2} \right)^2 \nabla \mathbf{d} \right) \right) + \tilde{A} \mathcal{A}_{\mathbf{u}} \right) = 0, \quad (3.4)$$

$$\nabla \cdot \mathbf{u} = 0, \quad (3.5)$$

$$\mathbf{u}|_{\partial\Omega} = 0, \quad \partial_n \phi|_{\partial\Omega} = 0, \quad \partial_n \mathbf{d}|_{\partial\Omega} = 0, \quad (3.6)$$

where the dimensionless groups are,

$$\begin{aligned} Re &= \frac{L^2 \rho}{\nu t_0}, \quad Er = \frac{L^2 \nu}{K t_0}, \quad \tilde{A} = \frac{A t_0}{\nu L^2}, \quad Ca = \frac{L^2 \nu}{\lambda t_0}, \\ \tilde{M}_1 &= M_1 \nu, \quad \tilde{M}_2 = M_2 \nu, \\ \tilde{\varepsilon} &= \frac{\varepsilon}{L}, \quad \tilde{F} = \frac{4}{(\tilde{\varepsilon})^2} (1 - \phi^2)^2, \quad \tilde{f} = \tilde{F}', \\ \tilde{\eta} &= \frac{\eta}{L}, \quad \tilde{G}(\mathbf{d}) = \frac{1}{4\tilde{\eta}^2} (\|\mathbf{d}\|^2 - 1)^2, \quad \tilde{g} = \tilde{G}'. \end{aligned} \quad (3.7)$$

Re is the Reynolds number, Er is the Ericksen number, Ca is the capillary number, \tilde{A} , \tilde{M}_1 and \tilde{M}_2 are the dimensionless analogs of M_1, M_2, A . To simplify the notation, we will drop all tildes from here on.

4. Numerical method

The purpose of this section is to develop an efficient numerical scheme for the coupled nonlinear system (3.1)–(3.5). Since we are primarily concerned with a spectral discretization, our guiding principle here is to design a simple, yet efficient and accurate numerical scheme by avoiding, as much as possible, solving problems with non-constant coefficients at each time step. Due to the complexity of the system, only first-order time discretization will be presented in detail, but a second-order version can also be designed (cf. [62,55]). We shall describe our approach for the phase equation, director field equation, and Navier–Stokes equations respectively before we describe the complete time discretization scheme for (3.1)–(3.6).

4.1. A stabilized time discretization scheme for the phase equation

Let us consider the Allen–Cahn equation with Lagrange multiplier to enforce the conservation of volume for each phase. Following [62,61,55,54,53], we use the stabilized semi-implicit scheme as follows.

$$\left(\frac{1}{\delta t} + \frac{S_1 M_1 \lambda}{\varepsilon^2}\right)(\phi^{n+1} - \phi^n) + (\mathbf{u}^n \cdot \nabla)\phi^n = \frac{M_1}{Ca}(\Delta\phi^{n+1} - f(\phi^n)) - \frac{M_1}{Er} \mathcal{K}_\phi^n - M_1 A \mathcal{A}_\phi^n + M_1 \zeta^{n+1}, \quad (4.1)$$

$$\frac{\partial\phi^{n+1}}{\partial n} \Big|_{\partial\Omega} = 0, \quad (4.2)$$

$$\int_{\Omega} \phi^{n+1} \mathbf{d}\mathbf{x} = \int_{\Omega} \phi^n \mathbf{d}\mathbf{x}, \quad (4.3)$$

where $\mathcal{K}_\phi^n = \frac{(1+\phi^n)^2}{2} \left(\frac{|\nabla\mathbf{d}^n|^2}{2} + G(\mathbf{d}^n)\right)$, \mathcal{A}_ϕ^n is the explicit treatment of the anchoring term and ζ^n is the Lagrange multiplier. In fact, from (4.3) we find

$$\zeta^{n+1} = \frac{1}{|\Omega|} \int_{\Omega} \left(\frac{1}{Ca} f(\phi^n) + \frac{1}{Er} \mathcal{K}_\phi^n + A \mathcal{A}_\phi^n\right) \mathbf{d}\mathbf{x}. \quad (4.4)$$

We recall that $f(\phi) = \frac{\phi(\phi^2-1)}{\varepsilon^2}$, so the explicit treatment of this term usually leads to a severe restriction on the time step δt when $\varepsilon \ll 1$. Thus we introduce in (4.1) an extra dissipative “*stabilizer*” term which is of order $\frac{S_1 \delta t}{\varepsilon^2}$, to improve stability while preserving simplicity of implementation.¹ The stabilizer allows us to treat the nonlinear term explicitly without time step constraints as shown in [62,61,55,54,53].

4.2. A stabilized time discretization scheme for the director field equation

To avoid solving a nonlinear equation at each time step while allowing reasonable time steps, we adopt the same strategy as above and propose the following stabilized semi-discrete numerical algorithm:

$$\begin{aligned} \left(\frac{1}{\delta t} + \frac{S_2 M_2 K}{\eta^2}\right)(\mathbf{d}^{n+1} - \mathbf{d}^n) + (\mathbf{u}^n \cdot \nabla)\mathbf{d}^n - \mathbf{W}^n \cdot \mathbf{d}^n &= \frac{M_2}{Er}(\Delta\mathbf{d}^{n+1} - \Delta\mathbf{d}^n) + \frac{M_2}{Er} \nabla \cdot \left(\frac{1+\phi^n}{2}\right)^2 \nabla\mathbf{d}^n \\ &\quad - \frac{M_2}{Er} \left(\frac{1+\phi^n}{2}\right)^2 \mathbf{g}(\mathbf{d}^n) - M_2 A \mathcal{A}_\mathbf{d}^n, \end{aligned} \quad (4.5)$$

$$\frac{\partial\mathbf{d}^{n+1}}{\partial n} \Big|_{\partial\Omega} = 0, \quad (4.6)$$

where $\mathcal{A}_\mathbf{d}^n$ is the explicit treatment of the anchoring term. We add another stabilizing term (associated with S_2) to balance the explicit treatment of the term $\mathbf{g}(\cdot)$.

4.3. A pressure-correction scheme for the Navier–Stokes equation

In order to decouple the computation of the pressure from velocity, a projection scheme (see, for instance, a recent review in [21]) is used for the Navier–Stokes equation. We use the first-order pressure correction scheme while treating the nonlinear terms explicitly. The scheme is given as follows.

$$\frac{\tilde{\mathbf{u}}^{n+1} - \mathbf{u}^n}{\delta t} + (\mathbf{u}^n \cdot \nabla)\mathbf{u}^n - \frac{1}{Re} \Delta\tilde{\mathbf{u}}^{n+1} + \nabla p^n + \frac{1}{Re} \nabla \cdot \left(\frac{1}{Ca} \mathcal{J}_\phi^n + \mathcal{J}^n + \frac{1}{Er} \mathcal{K}_\mathbf{d}^n + A \mathcal{A}_\mathbf{u}^n\right) = 0, \quad (4.7)$$

¹ It is the same order as the error introduced by the explicit treatment of $f(\phi)$. We refer to [54] for a more detailed discussion.

$$\tilde{\mathbf{u}}^{n+1}|_{\partial\Omega} = 0, \tag{4.8}$$

and

$$\frac{\mathbf{u}^{n+1} - \tilde{\mathbf{u}}^{n+1}}{\delta t} + \nabla(p^{n+1} - p^n) = 0, \tag{4.9}$$

$$\nabla \cdot \mathbf{u}^{n+1} = 0, \tag{4.10}$$

$$\mathbf{n} \cdot \mathbf{u}^{n+1}|_{\partial\Omega} = 0, \tag{4.11}$$

where \mathcal{J}_ϕ^n , \mathcal{S}^n , $\mathcal{K}_\mathbf{d}^n$ and $\mathcal{A}_\mathbf{u}^n$ are stress terms treated explicitly.

4.4. The complete time discretization for the coupled system

We next describe the complete first-order scheme for (3.4), (3.6). Given $(\mathbf{u}^n, p^n, \phi^n, \mathbf{d}^n)$, we update $(\mathbf{u}^{n+1}, p^{n+1}, \phi^{n+1}, \mathbf{d}^{n+1})$ as follows:

- (i) update ϕ^{n+1} from (4.1)–(4.3);
- (ii) update \mathbf{d}^{n+1} from (4.5) and (4.6);
- (iii) update $\tilde{\mathbf{u}}^{n+1}$ from (4.7) and (4.8), then update $\mathbf{u}^{n+1}, p^{n+1}$ from (4.9)–(4.11).

Remark 1. We have introduced in (4.1) and (4.5) extra dissipative terms of order $S_1 \frac{dt}{\epsilon^2}$ and $S_2 \frac{dt}{\eta^2}$, respectively, to improve stability while preserving simplicity of implementation. The parameters S_1 and S_2 are proportional to the amount of artificial dissipation added in the numerical scheme. Larger S_1 and S_2 will lead to a more stable but less accurate scheme. Extensive numerical experiments indicate that the choice of $S_1 = S_2 = 2$ in Cartesian coordinates and $S_1 = S_2 = 5$ in cylindrical coordinates provides a good balance between stability and accuracy.

4.5. Spatial discretization

We emphasize that the scheme described above leads to, at each time step, a sequence of Helmholtz equations, which can be discretized with any proper spatial discretization, in particular FFT solvers. In numerical simulations, after we pre-assign the interfacial width ϵ , the grid resolution is decided to ensure resolution for the interfacial width, and the time step is set to obtain the desirable accuracy (i.e., the time step is small enough to get convergence.) Since we plan to simulate drop formation and pinch-off in a cylindrical axisymmetric domain, we use the Legendre–Galerkin method (cf. [50,51]). For more details on the Legendre–Galerkin method for solving the vector (for the velocity and director) and scalar (for the pressure and phase function) Helmholtz equation in a cylindrical axisymmetric geometry, we refer to [37,62].

5. Numerical simulations

We now present simulation results on numerical benchmarks related to filament breakup and drop formation, and then we extend the simulations to anisotropic viscoelasticity (i.e., a liquid crystal phase). Our phase field formulation and numerical algorithms generalize the classical problem of two-phase immiscible viscous fluids, in that we can pass to the two phase Newtonian fluid limit by setting $\frac{1}{Er} = A = 0$ in system (3.4), (3.6). Thus we have the capability to numerically explore the competition between capillary forces, gravity, nematic distortional elasticity, and LC interfacial anchoring in filament thinning, drop pinch-off and drop deformation behavior. In this paper, we will only sample this competition to illustrate the modeling and numerical advances, deferring a complete phase diagram of filament and drop phenomena to a sequel.

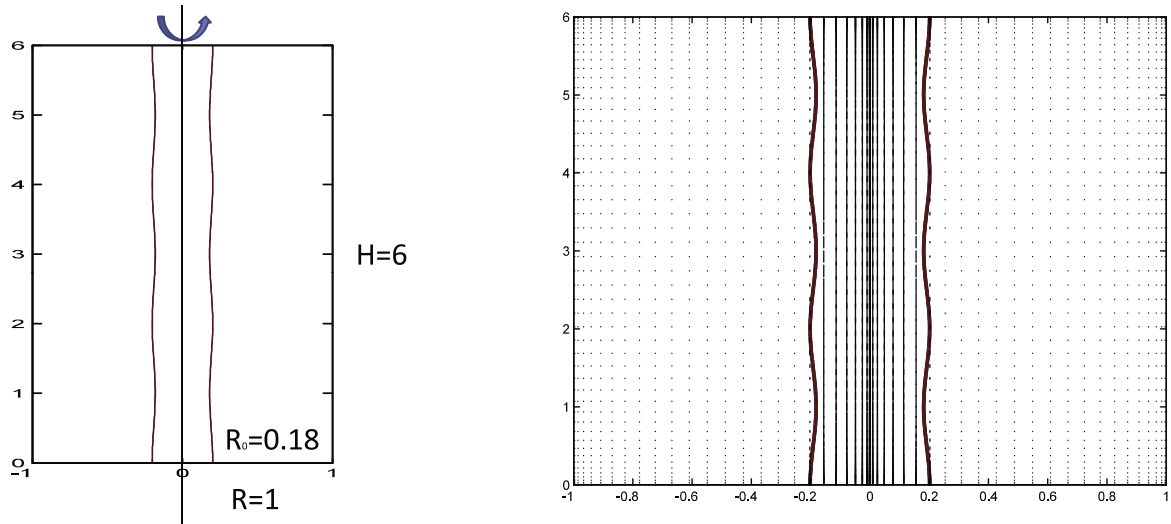
In simulations, the computational domain is a cylinder of radius of R and height $H = 6R$ with $R = 1$. We impose axisymmetry so the computational domain is a “rectangle” in (r, z) space: $\Omega = \{(r, z) : r \in (0, R), z \in (0, 6R)\}$. We fix $Re = 1$, $Ca = 10$, and fix the following model and numerical parameters:

$$M_1 = 0.01, M_2 = 0.0001, \epsilon = 0.01, \eta = 0.03, \delta t = 0.0001. \tag{5.1}$$

The initial velocity is set to zero. We have taken special effort to ensure that numerical solutions are well resolved in space (512×512 grid points) and time with a sufficiently small time step.

5.1. Dynamics of viscous and nematic liquid crystal filaments

We first simulate the evolution of the Rayleigh instability for a viscous cylindrical filament of radius $R_0 = 0.18R$ and height $H_0 = 6R$ centered around the axis of a cylinder of radius R and height $H = 6R$. The rest of the cylinder is filled with an immiscible ambient fluid (see the first plot in Fig. 5.1) of the same viscosity and density. We superimpose a small pertur-



(a) Initial profile of the level set $\phi = 0$ for the filament boundary.

(b) Initial profile of the LC director field \mathbf{d} within the filament.

Fig. 5.1. The initial filament interface and director field: $\phi(t = 0) = 0, \mathbf{d}(t = 0)$.

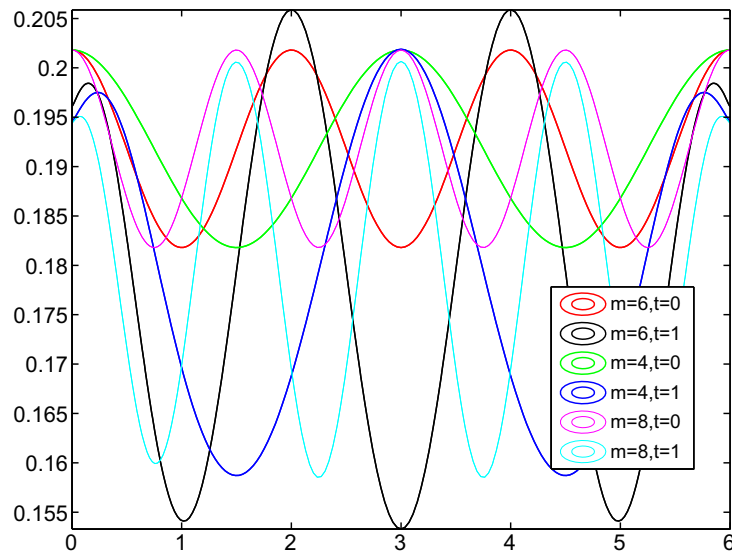


Fig. 5.2. The contours lines of $\{\phi = 0\}$ for different wave numbers.

bation (of amplitude θ_0 and wavenumber $\omega_m = \frac{m\pi}{H}$) to the cylindrical filament by initializing the zero level set of the labeling function, ϕ_0 , as follows.

$$\phi_0(r, z) = -\tanh\left(\left(\frac{r^2}{(R_0 + \theta_0 \cos(\omega_m z))^2} - 1\right) \frac{R_0^2}{\varepsilon}\right), \quad (5.2)$$

$$\mathbf{d}_0(r, z) = (\mathbf{d}_0^r, \mathbf{d}_0^z) = \left(0, \left(\frac{1 + \phi_0}{2}\right)^2\right). \quad (5.3)$$

In the above initial data, we set $\theta = 0.1, \omega_m = \frac{m\pi}{H}$ where m labels the discrete wave number. For fully nonlinear simulations, we seed the fastest growing discrete wavenumber mode in the initial data. Fig. 5.2 show the comparisons of zero level sets (the filament "interface") of the phase field function $\{\phi = 0\}$ from snapshots at $t = 0$ and $t = 1$ for $m = 4, 6, 8$, for the viscous limit of our model (2.14), i.e., $\frac{1}{\varepsilon} = A = 0$.

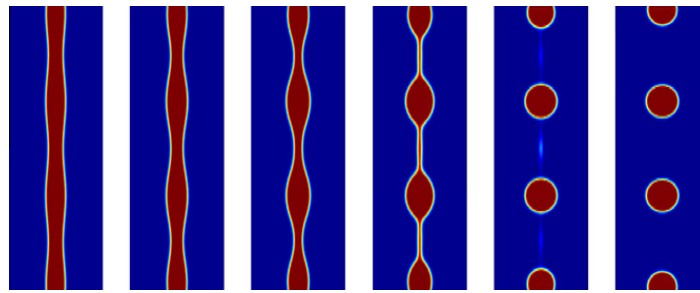


Fig. 5.3. Viscous filament dynamics: The onset and saturation of the Rayleigh instability for a viscous filament in a viscous ambient fluid of the same density and viscosity. Snapshots are presented at $t = 2, 3, 4, 5, 6, 7$.

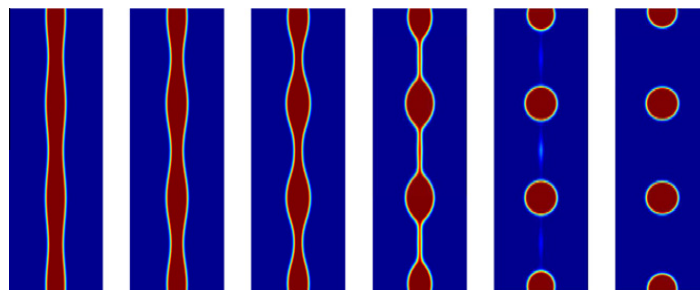


Fig. 5.4. Liquid crystal filament dynamics with weak Frank elasticity, $Er = 10^4$, and zero anchoring energy, $A = 0$. Frank elasticity modifications to the viscous filament dynamics. Snapshots at $t = 2, 3, 4, 5, 6, 7$ with identical parameters to Fig. 5.3 except nonzero Er .

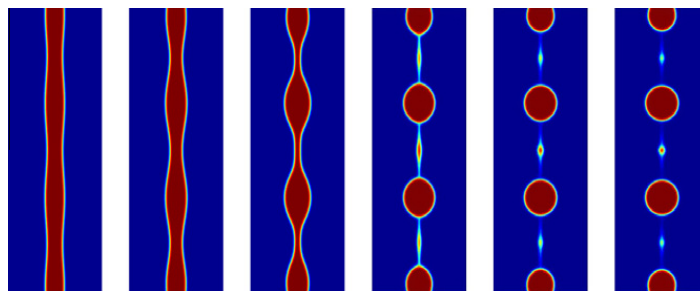


Fig. 5.5. Liquid crystal filament dynamics with increased Frank elasticity, $Er = 100$, relative to Fig. 5.4, and zero anchoring energy, $A = 0$. Snapshots are presented at $t = 1, 2, 3, 3.7, 3.9, 4$.

We first show the classical dynamics of a purely viscous fluid filament, simulated with $\frac{1}{Er} = A = 0$; and then compare the viscous results with a LC filament with varying strength of Frank elasticity, first without interfacial anchoring energy ($A = 0$) and later with weak anchoring that biases tangential interfacial orientation.

Viscous filament dynamics ($\frac{1}{Er} = A = 0$): Fig. 5.3. The imposed perturbation grows, creating thin “necks”, which continue to thin. At $t = 5$, four beads have formed, connected by thin threads that continue to thin and then rupture before $t = 6$; note the drops consume all fluid from the thin filaments. It is noteworthy that the satellite drop radii are uniform, owing to viscous fluid dynamics and the symmetry of the imposed perturbation. This simulation captures the onset and nonlinear saturation of the classical Rayleigh instability [15] (sufficiently long wavelength capillary waves grow in amplitude, leading to pinch-off at the nodes of the waveform).

“Weakly elastic” liquid crystal filament dynamics with zero interfacial anchoring energy: Fig. 5.4. We change only the Frank elastic constant from zero to $K = 10^{-13}$ Newtons (typical of nematic liquid crystals) and select observational timescale $t_0 = 1s$, lengthscale $L = 10^{-3}m$, and kinematic viscosity $\nu = 10^{-3}Pa.s$, or equivalently, Ericksen number $Er = \frac{L^2\nu}{Kr_0} = 10^4$. We retain zero anchoring energy, $A = 0$, and the other parameters from Fig. 5.3. Since the bulk elastic constant is very small, the dynamics of the liquid crystal filament is perturbative of the viscous filament simulation.

Liquid crystal filament dynamics with stronger Frank elasticity and zero interfacial anchoring energy: Fig. 5.5. We now increase Frank elasticity by lowering the Ericksen number to $Er = 100$, keeping zero anchoring energy, $A = 0$. This simulation focuses on the coupling of elastic distortions to the hydrodynamics of the Rayleigh instability, isolated from the equally important role of anchoring energy at the filament-ambient interface. The model predicts a significant influence, with sec-

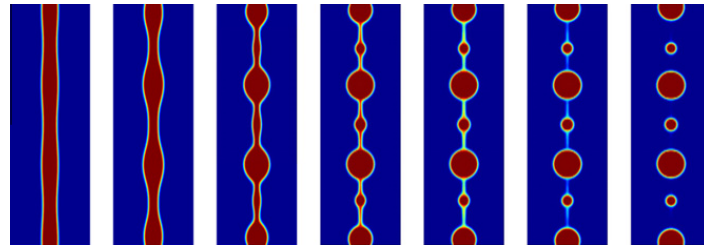


Fig. 5.6. Liquid crystal filament dynamics with increased Frank elasticity, $Er = 1$, relative to $Er = 100$ of Fig. 5.5, and zero anchoring energy, $A = 0$. Snapshots are shown at $t = 1, 2, 2.6, 3, 3.2, 3.5, 4$.

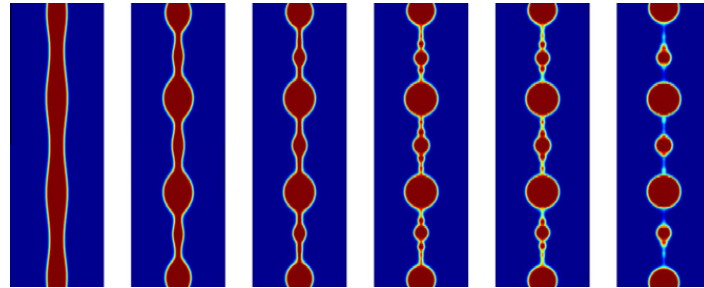


Fig. 5.7. Liquid crystal filament dynamics with increased Frank elasticity, $Er = 1/3$, relative to $Er = 1$ of Fig. 5.6, and zero anchoring energy, $A = 0$. Snapshots are taken at $t = 1, 1.5, 1.6, 1.8, 1.9, 2.3$.

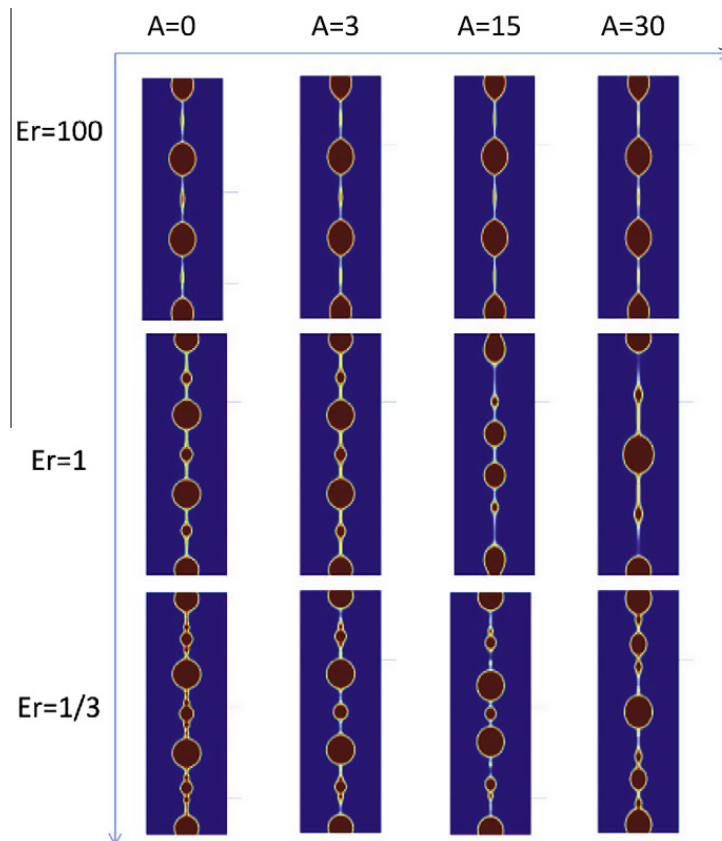
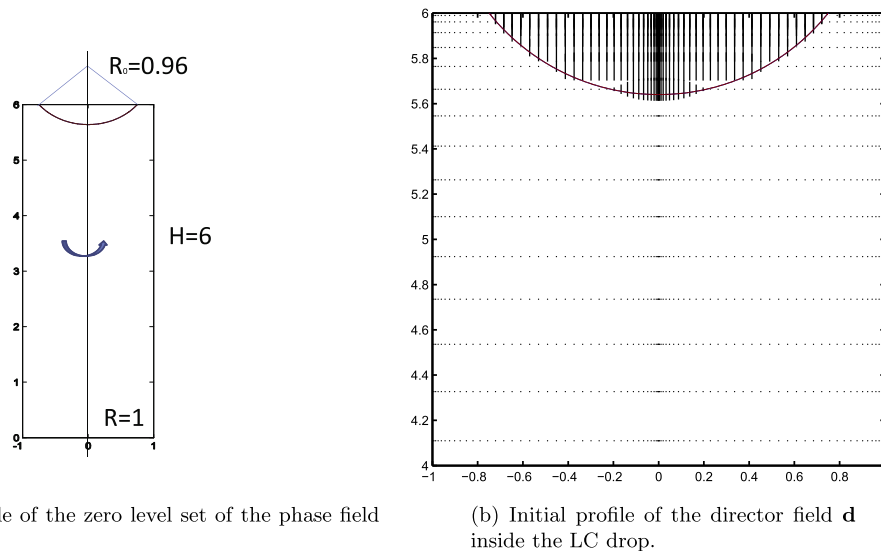


Fig. 5.8. LC filament evolution prior to satellite formation with surface anchoring energy values $A = 0, 3, 15, 30$ and Ericksen numbers $Er = 100, 1, 1/3$. A snapshot comparison of LC filament evolution. From left to right, the snapshots are taken at $t = 3.7, 4, 4, 4$ in the first row, $t = 3.2, 3.5, 6.4, 8.4$ in the second row, $t = 1.8, 2.2, 3, 3.4$ in the third row.

ondary satellite drop formation within the thin filament connecting the primary satellite drops instead of the fluid in the filaments draining back into the primary satellite drops.

Liquid crystal filament dynamics with yet stronger Frank elasticity, $Er = 1$, and zero anchoring energy $A = 0$: Fig. 5.6. We amplify Frank elastic energy (by lowering the Ericksen number to $Er = 1$), while continuing to suppress anchoring energy, $A = 0$.



(a) Initial profile of the zero level set of the phase field function ϕ .

(b) Initial profile of the director field \mathbf{d} inside the LC drop.

Fig. 5.9. Initial profiles of the zero level set of the labeling function $\{\phi = 0\}$ and the director field \mathbf{d} .

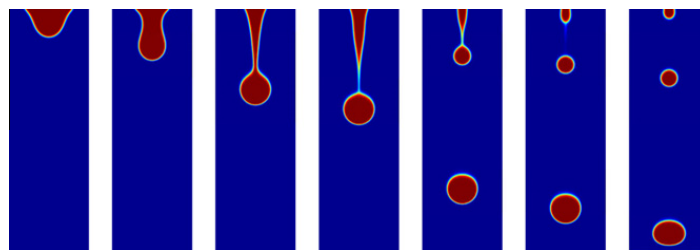


Fig. 5.10. Snapshots of a viscous dripping faucet simulation at $t = 1, 2, 3, 3.4, 5, 5.4, 6$.

The beads-on-a-string phenomenon persists with the most noticeable effect that the secondary satellite drops contain more fluid volume. One is led to wonder how close we can tune the primary and secondary drop radii by further raising Frank elastic energy, explored in the next simulation.

Liquid crystal filament dynamics with more enhanced Frank elasticity, $Er = 1/3$, and zero anchoring energy $A = 0$: Fig. 5.7. Here we find the previous scenarios for $Er = 100$ and $Er = 1$ do not persist; instead, a tertiary instability arises in the threads between the primary and secondary satellite drops. These results combine to suggest that the competition between gravity, capillarity and nematic (Frank) elastic stress can lead to polydisperse droplet streaming from a single filament, without noisy input from the ambient. Of course, these predictions are void of the important effects of nematic surface anchoring typical of most LC interfaces, which we explore next.

Liquid crystal filament dynamics with variable Frank elasticity and variable interfacial anchoring energy: Fig. 5.8. As a final illustration of the model predictions, we incorporate LC surface anchoring energy to three of the simulations above, varying the anchoring strength parameter from $A = 0$ to $A = 3, 15, 30$ for $Er = 100, 1, 1/3$. Fig. 5.8 shows selected snapshots for each of the nine new simulations along side a comparable snapshot with $A = 0$. These results do not lend themselves to a definitive phase diagram, but certain local trends are evident within the table of snapshots. The physical implications of these snapshots, including polydispersity of satellite drop formation and the role of defects in these filament and droplet morphologies, will be pursued in a sequel.

5.2. The leaking nematic liquid crystal faucet

In the section, we consider a nematic liquid crystal drop under the influence of gravity, falling from a nozzle with an initial spherical shape (Fig. 5.9a) and and director field \mathbf{d} (Fig. 5.9b). The boundary conditions for \mathbf{u} , ϕ , and \mathbf{d} are adopted from the previous section, with zero velocity at the mouth of the “nozzle”. The initial profiles of the phase field function ϕ and director field \mathbf{d} are given, respectively, by:

$$\phi_0(r, z) = \tanh \left(\frac{R_0^2 - r^2 - (z - H - 0.6)^2}{\varepsilon} \right), \quad (5.4)$$

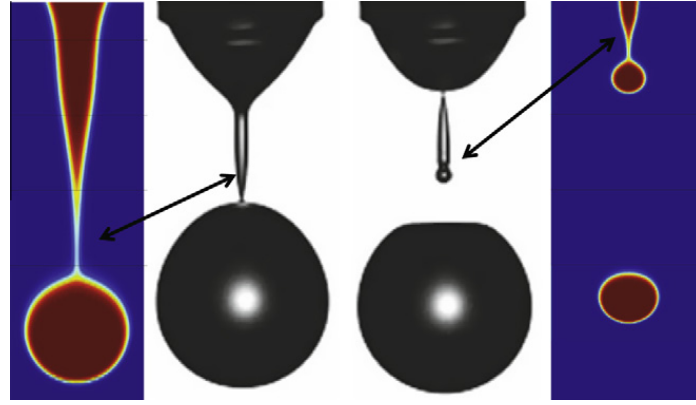


Fig. 5.11. Qualitative comparison between the experimental benchmark [57] of two-phase viscous fluids (50% glycerol in water) and our Fig. 5.10 results for the viscous dripping faucet at $t = 3.4, 5$.

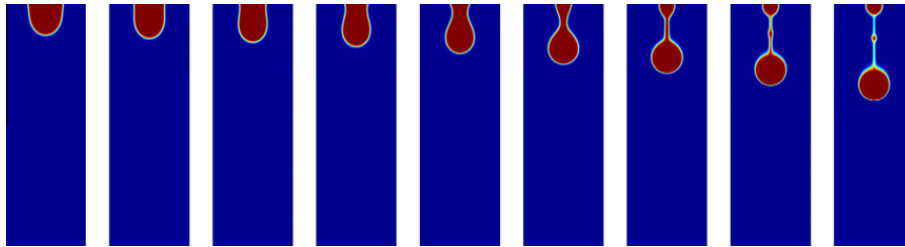


Fig. 5.12. Snapshots of the leaking liquid crystal faucet into a viscous, slightly less dense, fluid, at $t = 4, 6, 8, 9, 9.6, 10, 10.2, 10.4, 10.6$ with Ericksen number $Er = 1$ and anchoring energy strength $A = 0$.

$$\mathbf{d}_0(r, z) = \left(0, \left(\frac{1 + \phi_0}{2} \right)^2 \right). \quad (5.5)$$

The director field is initially given uniform alignment in the direction of gravity.

We consider the case where the density difference of the liquid crystal drop and ambient fluid is small so that we can use the Boussinesq approximation [35,62] to derive the momentum balance equation for a mixture with small density variation. The momentum equation is given by

$$\rho_0(\mathbf{u}_t + (\mathbf{u} \cdot \nabla)\mathbf{u}) = -\nabla p + \nabla \cdot \boldsymbol{\sigma} + f_{\text{gty}}\mathbf{e}_z, \quad (5.6)$$

where $\mathbf{e}_z = (0, 0, 1)^T$, $f_{\text{gty}} = -((1 + \phi)(\rho_1 - \rho_0) + (1 - \phi)(\rho_2 - \rho_0))g_0$, g_0 is the gravity acceleration. In dimensionless form, it is

$$(\mathbf{u}_t + (\mathbf{u} \cdot \nabla)\mathbf{u}) = -\nabla p + \nabla \cdot \boldsymbol{\sigma} - \left[\left((1 + \phi) \left(\frac{\rho_1}{\rho_0} - 1 \right) + (1 - \phi) \left(\frac{\rho_2}{\rho_0} - 1 \right) \right) \frac{1}{Fr} \right] \mathbf{e}_z \quad (5.7)$$

where $Fr = \frac{1}{g_0}$ is the Froude number. We set $\frac{\rho_1}{\rho_0} = 0.5$, $\frac{\rho_2}{\rho_0} = 1.5$, and $\frac{1}{Fr} = 10$.

We compare nematic liquid crystal and viscous dripping faucets. For simplicity, we only consider Frank elastic energy and suppress anchoring energy for the purposes of this paper.

The viscous falling droplet benchmark, Fig. 5.10. When the drop is sufficiently massive, gravity overcomes surface tension and the drop begins to droop. The classical scenario unfolds (Fig. 5.10): necking, formation of a drop at the tip, a thin filament forms between the elongated fluid attached to the faucet and the emerging satellite drop, and the thread breaks leading to drop pinch-off. If the original mass is sufficiently large that the remaining fluid attached to the faucet does not recoil under surface tension, then the above scenario repeats itself until the faucet fluid mass can no longer fall. These viscous simulations are qualitatively consistent with experimental results in [57] (Fig. 5.11).

Frank elasticity effects on the dripping faucet, Fig. 5.12 To illustrate the model and numerical algorithm, we simulate the leaking liquid crystal faucet with an Ericksen number $Er = 1$ and suppressed anchoring energy (Fig. 5.12). The Frank elastic stress leads to formation of a persistent, long thread connecting the nematic LC mass at the faucet and the LC drop that forms at the leading edge of the falling fluid mass. Furthermore, the thread does not break in the timescales shown here, and a smaller satellite drop forms instead that starts to look similar to the filament stretching scenarios reported above. Again, a more complete inquiry into the details of the nematic LC physics and different scenarios possible by varying both the Frank elastic energy and anchoring energy is deferred to a sequel.

6. Concluding remarks

In this paper, we derive an energetic phase-field model for two-phase complex fluids with one liquid crystal phase and another viscous fluid phase. The continuum model obeys an energy dissipation law, which yields a conditionally stable, accurate, and relatively easy to implement, numerical scheme. In particular, we developed a stable semi-implicit time-marching scheme coupled with a Legendre–Galerkin discretization in space for the fully coupled system. With this numerical scheme, we conduct two benchmark numerical experiments for interfacial fluid flows. The first simulation probes the onset and non-linear dynamics of a weakly perturbed liquid crystal filament in an ambient viscous fluid of the same density and viscosity. The second simulation is of the leaky liquid crystal faucet into a slightly less dense viscous fluid. The model and code admit a viscous two-phase fluid limit, which is simulated first to compare with classical results both numerical and experimental. We then explore the coupling of Frank elastic energy to gravity and capillary forces for both benchmark problems, and for the filament stretching problem we likewise explore the effects of tangential interfacial anchoring energy at the LC-viscous fluid interface. Further investigations into liquid crystal physics and phase diagrams of droplet polydispersity, as well as schemes for higher density and viscosity contrasts, are deferred to future studies.

Acknowledgments

The authors thank Professor Jimmy Feng for stimulating discussions and insightful comments. The respective research of the authors is partially supported as follows: Forest, Wang and Yang by NSF DMS 1200487 and DMR 1122483 and CMMI 0819051, AFOSR FA9550 11–1-0328 and 12–1-0178; Shen by NSF-0915066 and AFOSR FA9550-11–1-0328; Li by NSFC-10971212 and NSFC-91130014; Liu by NSF-1159937 and 1109107; and Chen by NKBRPC-2011CB302400 and NSFC-11031007.

References

- [1] Lab Chip. 4, 2004.
- [2] G. Gonnella, A. Lamura, J.M. Yeomans, Europhys. Lett. 45 (1999) 314.
- [3] D. Adalsteinsson, J.A. Sethian, A fast level set method for propagating interfaces, J. Comput. Phys. 118 (1995) 269–277.
- [4] D.M. Anderson, G.B. McFadden, A.A. Wheeler, Diffuse-interface methods in fluid mechanics, Annu. Rev. Fluid Mech. 30 (1998) 139–165.
- [5] V.L. Berdichevsky, Variational principles of continuum mechanics: I Fundamentals, Springer, Interaction of Mechanics and Mathematics, 2009.
- [6] P. Bhat, S. Appathurai, M.T. Harris, M. Pasquali, G.H. McKinley, O.A. Basaran, Formation of beads-on-a-string structures during break-up of viscoelastic filaments, Nature Phys. 6 (2010) 625–631.
- [7] B.R. Bird, C.F. Curtiss, R.C. Armstrong, O. Hassager, Dynamics of Polymeric Liquids, 2 Volume Set, Wiley & Sons, Inc., 1994.
- [8] Y. Brenier, The least action principle and the related concept of generalized flows for incompressible perfect fluids, J. Am. Math. Soc. 2 (1989) 225.
- [9] J.W. Cahn, J.E. Hilliard, Free energy of a nonuniform system, I interfacial free energy, J. Chem. Phys. 28 (1958) 258–267.
- [10] S. Chen, G.D. Doolen, Lattice boltzmann method for fluid flows, Annu. Rev. Fluid Mech. 30 (1998) 329.
- [11] R. Cohen, R. Hardt, D. Kinderlehrer, S-Y. Lin, M. Luskin, Minimum energy configurations for liquid crystals: computational results, Theory Appl. Liq. Cryst. 1340 (1988) 123–138.
- [12] D. Coutand, S. Shkoller, Well-posedness of the full Ericksen–Leslie model of nematic liquid crystals, C. R. Acad. Sci. Paris series I (2001) 919–924.
- [13] V. Cristini, Y-C. Tan, Theory and numerical simulation of droplet dynamics in complex flows – a review, Lab Chip 4 (2004) 257–264.
- [14] P.-G. de Gennes, J. Prost, The Physics of Liquid Crystals, Oxford University Press, New York, 1993.
- [15] P.G. Drazin, W.H. Reid, Hydrodynamic Stability, Cambridge University Press, New York, 1981.
- [16] Q. Du, M. Li, C. Liu, Analysis of a phase field Navier-Stokes vesicle-fluid interaction model, DCDS-B 8 (3) (2007) 539–556.
- [17] J.L. Ericksen, Anisotropic fluids, Arch. Rat. Mech. Anal. 4 (1960) 231–237.
- [18] J.L. Ericksen, Liquid crystals with variable degree of orientation, IMA Preprint Series, 1989, pp. 559.
- [19] J.J. Feng, C. Liu, J. Shen, P. Yue, An energetic variational formulation with phase field methods for interfacial dynamics of complex fluids: advantages and challenges, IMA Vol. Math. Appl. 140 (2005) 1–26.
- [20] J. Glimm, M.J. Graham, J. Grove, X.L. Li, T.M. Smith, D. Tan, F. Tangerman, Q. Zhang, Front tracking in two and three dimensions, J. Comput. Math. 7 (1998) 1–12.
- [21] J.L. Guermond, P. Mineev, J. Shen, An overview of projection methods for incompressible flows, Comput. Methods Appl. Mech. Engrg. 195 (2006) 6011–6045.
- [22] M.E. Gurtin, D. Polignone, J. Vinals, Two-phase binary fluids and immiscible fluids described by an order parameter, Math. Models Methods Appl. Sci. 6 (6) (1996) 815–831.
- [23] B.D. Hamlington, B. Steninhaus, J.J. Feng, D. Link, M.J. Shelley, A.Q. Shen, Liquid crystal droplet production in a microfluidic device, Liquid Cryst. 34 (2007) 861–870.
- [24] C.W. Hirt, B.D. Nichols, Volume of fluid method for the dynamics of free boundaries, J. Comput. Phys. 39 (1) (1981) 201–225.
- [25] T.Y. Hou, Numerical study of free interface problems using boundary integral methods, Documenta Mathematica, Extra Volume – Proceedings of the International Congress of Mathematicians III (1998) 601–610.
- [26] J. Janik, R. Tadmor, J. Klein, Shear of molecularly confined liquid crystals, 1 orientation and transitions under confinement, Langmuir 13 (1997) 4466–4473.
- [27] B. Jerome, Surface effects and anchoring in liquid crystals, Rep. Prog. Phys. 54 (1991) 391.
- [28] D. Khismatullin, Y. Renardy, M. Renardy, Development and implementation of VOF-PROST for 3d viscoelastic liquid-liquid simulations, J. Non-Newt. Fluid Mech. 140 (1992) 120–131.
- [29] R.G. Larson, The Structure and Rheology of Complex Fluids, Oxford University Press, 1999.
- [30] F.M. Leslie, Some constitutive equations for anisotropic fluids, Q. J. Mech. Appl. Math. 19 (1966) 357–370.
- [31] F.H. Lin, On nematic liquid crystals with variable degree of orientation, Commun. Pure Appl. Math. 44 (1991) 453–468.
- [32] F.H. Lin, Mathematical theory of liquid crystals, in: Applied Mathematics at the Turn of Century: Lecture notes of the 1993 Summer School, Universidad Complutense de Madrid, 1995.
- [33] F.H. Lin, C. Liu, Nonparabolic dissipative systems modeling the flow of liquid crystals, Commun. Pure Appl. Math. 48 (1995) 501–537.
- [34] F.H. Lin, C. Liu, Static and dynamic theories of liquid crystals, J. Part. Diff. Equat. 14 (2001) 289–330.
- [35] C. Liu, J. Shen, A phase field model for the mixture of two incompressible fluids and its approximation by a Fourier-spectral method, Physica D 179 (3–4) (2003) 211–228.

- [36] C. Liu, N.J. Walkington, An Eulerian description of fluids containing visco-hyperelastic particles, *Arch. Rat. Mech. Anal.* 159 (2001) 229–252.
- [37] J.M. Lopez, J. Shen, An efficient spectral-projection method for the Navier+Stokes equations in cylindrical geometries I. Axisymmetric cases, *J. Comput. Phys.* 139 (1998) 308–326.
- [38] J. Lowengrub, J. Goodman, H. Lee, E. Longmire, M. Shelley, L. Truskinovsky, in: I. Athanopoulos, M. Makrakis, J.F. Rodrigues (Eds.), *Free Boundary Problems: Theory and Applications*, CRC Press, London, 1999, p. 221.
- [39] J. Lowengrub, L. Truskinovsky, Quasi-incompressible Cahn-Hilliard fluids and topological transitions, *R. Soc. Lond. Proc. Ser. A: Math. Phys. Eng. Sci.* 454 (1978) (1998) 2617–2654.
- [40] O. Harlen, N. Morrison, Viscoelasticity in inkjet printing, *Rheol. Acta* 49 (2010) 619–632.
- [41] R.R. Nourgaliev, T.N. Dinh, T.G. Theofanous, D. Joseph, *Int. J. Multiphase Flow* 29 (2003) 117.
- [42] L. Onsager, Reciprocal relations in irreversible processes I, *Phys. Rev.* 37 (1931) 405–426.
- [43] L. Onsager, Reciprocal relations in irreversible processes, II, *Phys. Rev.* 38 (1931) 2265–2279.
- [44] S.J. Osher, A level set formulation for the solution of the Dirichlet problem for Hamilton-Jacobi equations, *SIAM J. Anal.* 24 (1993) 1145–1152.
- [45] C.S. Peskin, The immersed boundary method, *Acta Numer.* 11 (2002) 1–39.
- [46] J.M. Rallison, The deformation of small viscous drops and bubbles in shear flows, *Ann. Rev. Fluid Mech.* 16 (1984) 45–66.
- [47] D.H. Rothman, S. Zaleski, *Lattice Gas Cellular Automata*, vol. 4, Cambridge University Press, Cambridge, 1997.
- [48] K. Sankaranarayanan, I.G. Kevrekidis, S. Sundaresan, J. Lu, G. Tryggvason, *Int. J. Multiphase Flow* 29 (2003) 109.
- [49] R. Sattler, S. Gier, J. Eggers, C. Wagner, The final stages of capillary break-up of polymer solutions, *Phys. Fluids* 24 (2012) 023101.
- [50] J. Shen, Efficient spectral-Galerkin method I. direct solvers for second- and fourth-order equations by using Legendre polynomials, *SIAM J. Sci. Comput.* 15 (1994) 1489–1505.
- [51] J. Shen, Efficient spectral-galerkin method III. polar and cylindrical geometries, *SIAM J. Sci. Comput.* 18 (1997) 1583–1604.
- [52] J. Shen, C. Liu, On liquid crystal flows with free-slip boundary conditions, *Dis. Cont. Dyn. Sys.* 7 (2001) 307–318.
- [53] J. Shen, X. Yang, Energy stable schemes for Cahn-Hilliard phase-field model of two-phase incompressible flows, *Chinese Ann. Math. Ser. B* 31 (2010) 743–758.
- [54] J. Shen, X. Yang, Numerical approximations of Allen-Cahn and Cahn-Hilliard equations, *DCDS, Ser. A* 28 (2010) 1169–1691.
- [55] J. Shen, X. Yang, A phase-field model and its numerical approximation for two-phase incompressible flows with different densities and viscosities, *SIAM J. Sci. Comput.* 32 (2010) 1159–1179.
- [56] H.A. Stone, Dynamics of drop deformation and break up in viscous fluids, *Ann. Rev. Fluid Mech.* 26 (1994) 65–102.
- [57] V. Tirtaatmadja, G.H. McKinley, J.J. Cooper-White, Drop formation and breakup of low viscosity elastic fluids: Effects of molecular weight and concentration, *Phys. Fluids* 18 (2006) 043101.
- [58] G. Tryggvason, B. Bunner, A. Esmaeeli, D. Juric, N. Al-Rawahi, W. Tauber, J. Han, S. Nas, Y.-J. Jan, A front-tracking method for the computations of multiphase flow, *J. Comput. Phys.* 169 (2) (2001) 708–759.
- [59] S. Veerapaneni, D. Gueyffier, G. Biros, D. Zorin, A boundary integral method for simulating the dynamics of inextensible vesicles suspended in a viscous fluid in 2d, *J. Comput. Phys.* 228 (7) (2009) 2334–2353.
- [60] T. Watanabe, K. Ebihara, *Comput. Fluids* 32 (2003) 823.
- [61] X. Yang, Error analysis of stabilized semi-implicit method of allen-cahn equation, *Disc. Conti. Dyn. Sys. B* 11 (4) (2009) 1057–1070.
- [62] X. Yang, J.J. Feng, C. Liu, J. Shen, Numerical simulations of jet pinching-off and drop formation using an energetic variational phase-field method, *J. Comput. Phys.* 218 (2006) 417–428.
- [63] X. Yang, M.G. Forest, C. Liu, J. Shen, Shear cell rupture of nematic liquid crystal droplets in viscous fluids, *J. Non-Newt. Fluid Mech.* 166 (2011) 487–499.
- [64] P. Yue, J.J. Feng, C. Liu, J. Shen, A diffuse-interface method for simulating two-phase flows of complex fluids, *J. Fluid. Mech.* 515 (2004) 293–317.
- [65] P. Yue, J.J. Feng, C. Liu, J. Shen, Viscoelastic effects on drop deformation in steady shear, *J. Fluid Mech.* 540 (2005) 427–437.
- [66] A.V. Zakhharova, Mitsumasa Iwamoto, Homeotropic-planar anchoring transition induced by trans-cis isomerization in ultrathin polyimide langmuir+cbldoggett films, *J. Chem. Phys.* 118 (2003) 10759–10761.